HHS Public Access

Author manuscript

Sci Transl Med. Author manuscript; available in PMC 2024 September 04.

Published in final edited form as:

Sci Transl Med. 2024 March 06; 16(737): eadk3868. doi:10.1126/scitranslmed.adk3868.

Inactivation of adenosine receptor 2A suppresses endothelial-to-mesenchymal transition and inhibits subretinal fibrosis in mice

Qiuhua Yang[1], **Yongfeng Cai**[1], **Qian Ma**[1], **Albert Xiong**[2], **Peishan Xu**[1], **Zhidan Zhang**[1], **Jiean Xu**[1], **Yaqi Zhou**[1], **Zhiping Liu**[1], **Dingwei Zhao**[1], **John Asara**[3], **Wei Li**[4], **Huidong Shi**[5,6], **Ruth B. Caldwell**[1,7], **Akrit Sodhi**[8], **Yuqing Huo**[1,7,*]

[1]Vascular Biology Center, Medical College of Georgia, Augusta University, Augusta, GA 30912, USA.

[2]Department of Ophthalmology, University of South Florida, Tampa, FL 33606, USA.

[3]Division of Signal Transduction, Beth Israel Deaconess Medical Center and Department of Medicine, Harvard Medical School, Boston, MA 02215, USA.

[4]Department of Ophthalmology, Cullen Eye Institute, Baylor College of Medicine, Houston, TX 77030, USA.

[5]Department of Biochemistry and Molecular Biology, Medical College of Georgia, Augusta University, Augusta, GA 30912, USA.

[6]Georgia Cancer Center, Medical College of Georgia, Augusta University, Augusta, GA 30912, USA.

[7]Department of Cellular Biology and Anatomy, Medical College of Georgia, Augusta University, Augusta, GA 30912, USA.

[8]Department of Ophthalmology, Wilmer Eye Institute, Johns Hopkins, Baltimore, MD 21287, USA.

Abstract

Anti–vascular endothelial growth factor therapy has had a substantial impact on the treatment of choroidal neovascularization (CNV) in patients with neovascular age-related macular degeneration (nAMD), the leading cause of vision loss in older adults. Despite treatment, many patients with nAMD still develop severe and irreversible visual impairment because of the development of subretinal fibrosis. We recently reported the anti-inflammatory and antiangiogenic effects of inhibiting the gene encoding adenosine receptor 2A (*Adora2a*), which has been implicated in cardiovascular disease. Here, using two mouse models of subretinal fibrosis (mice with laser injury–induced CNV or mice with a deficiency in the very low–density lipoprotein receptor),

*Corresponding author. yhuo@augusta.edu.

Author contributions: Q.Y. and Y.H. designed the study. Q.Y., Q.M., and J.A. performed a metabolomic assay. Q.Y., Q.M., and P.X. performed isolation, culture, and identification of mCECs. Q.Y., A.X., P.X., and D.Z. performed laser injury model and eye function assessment. Q.Y., P.X., J.X., Y.Z., Z.L., and D.Z. generated genetic mice. Q.Y., P.X., and Z.Z. treated mice with tamoxifen and KW6002. Q.Y., Y.C., A.X., J.X., Y.Z., and Z.L. performed the remainder of the imaging and data collection. Z.Z. and H.S. reanalyzed the public microarray data. Q.Y., Y.C., R.B.C., A.S., and Y.H. analyzed the data. Q.Y. and Y.H. wrote the manuscript. J.A., W.L., H.S., R.B.C., and A.S. critically reviewed and revised the manuscript. Q.Y., R.B.C., A.S., and Y.H. provided the reagents or materials and participated in designing the experiments.

Competing interests: The authors declare that they have no competing interests.

we found that deletion of *Adora2a* either globally or specifically in endothelial cells reduced subretinal fibrosis independently of angiogenesis. We showed that *Adora2a*-dependent endothelial-to-mesenchymal transition contributed to the development of subretinal fibrosis in mice with laser injury–induced CNV. Deficiency of *Adora2a* in cultured mouse and human choroidal endothelial cells suppressed induction of the endothelial-to-mesenchymal transition. A metabolomics analysis of cultured human choroidal endothelial cells showed that *ADORA2A* knockdown with an siRNA reversed the increase in succinate because of decreased succinate dehydrogenase B expression under fibrotic conditions. Pharmacological inhibition of ADORA2A with a small-molecule KW6002 in both mouse models recapitulated the reduction in subretinal fibrosis observed in mice with genetic deletion of *Adora2a*. ADORA2A inhibition may be a therapeutic approach to treat subretinal fibrosis associated with nAMD.

INTRODUCTION

Neovascular age-related macular degeneration (nAMD) is a retinal disorder that accounts for 90% of AMD-related vision loss (1–4). In patients with nAMD, an end-stage fibrous plaque/disciform scar that progresses from choroidal neovascularization (CNV) can cause profound and irreversible visual impairment (5–8). Subretinal fibrosis prevents retinal visual function because of its disruption of the highly organized retinal anatomical layers that tightly coordinate cellular interactions. Thus, therapeutic strategies for preventing or inhibiting subretinal fibrosis are imperative to improve visual outcomes in these patients.

Myofibroblasts contributing to the formation of subretinal fibrosis are transdifferentiated from various cells through a process known as mesenchymal or myofibroblast transition (9, 10). These cellular transitions include endothelial-to-mesenchymal transition (EndMT), macrophage-to-myofibroblast transition (MMT), and epithelial-to-mesenchymal cell transition (EMT) (11, 12). Increasing evidence suggests that endothelial cells (ECs) undergo EndMT under pathological circumstances and that EndMT contributes to various pathological fibrosis. EndMT also participates in the formation of retinal fibrosis. Analysis of epiretinal membranes from patients with proliferative diabetic retinopathy (PDR) has shown that ECs differentiate into myofibroblasts in the diabetic eye and contribute to pathologic fibrosis in PDR (13). The contribution of EndMT has also been demonstrated in a laser-induced mouse CNV model (14, 15). EndMT is regulated by a complex orchestration of several signaling pathways that are initiated by transforming growth factor β (TGFβ), proinflammatory cytokines, reactive oxygen species (ROS), and various transcriptional factors (16).

Adenosine receptor 2A (*ADORA2A* for human gene/*Adora2a* for rodent gene) is one of four G protein–coupled adenosine receptors (A1R, A2AR, A2BR, and A3R) that are highly expressed in the striatum of the brain, immune cells, and blood vessels (17, 18). ADORA2A activation stimulates the cyclic adenosine monophosphate (AMP)–protein kinase A (PKA) pathway by coupling to G_{olf} protein in peripheral tissues or G_s protein in the brain (19–21). In peripheral tissues of rodents, *Adora2a* has been reported to play a crucial role in the modulation of inflammation, myocardial oxygen consumption, coronary blood flow, angiogenesis, and control of cancer pathogenesis (22). We have reported that *Adora2a*

knockout/blockade promotes anti-inflammatory and antiangiogenic effects (23–25). In the current study, we hypothesized that deletion or blocking Adora2a could suppress the formation of subretinal fibrosis through inhibiting EndMT induction.

RESULTS

ADORA2A expression is associated with subretinal fibrosis in human and rodent AMD

To investigate the role of ADORA12A in ocular fibrotic diseases, we analyzed a microarray dataset (GSE60436) from fibrovascular membranes (FVMs) in patients with PDR (26). The results showed that *ADORA2A* gene expression was higher in active FVMs compared with normal retinas, along with increased expression of collagen family and matricellular proteins (Fig. 1A). To further examine the histopathology of the fibrotic area in eyes with AMD, we obtained paraffin-embedded eyes from patients with wet AMD and stained them with antibodies against ADORA2A and ACTA2. The results showed a strong expression of ADORA2A in the ACTA2-positive subretinal area of eyes from patients with wet AMD compared with eyes from healthy individuals (Fig. 1, B and C, and table S1). These findings demonstrated that ADORA2A was abundantly expressed in fibrotic tissue from areas of ocular degeneration diseases.

We next examined ADORA2A expression in laser-induced CNV lesions in mice, which is a model for subretinal fibrosis (9, 27, 28). In this model, we observed that CNV lesion size (IB4, CNV marker, red color) reached a maximum on day 7 and then regressed; CNV lesions almost completely disappeared by day 35. During the same period, subretinal fibrosis (indicated by COL1, a fibrosis marker in purple, and ACTA2, a myofibroblast/mesenchymal cell marker in green) was detected from days 7 to 35, with maximal size of subretinal fibrosis from days 21 to 35 (fig. S1). We therefore collected eyes from mice at days 7, 21, and 35 after laser injury and isolated the retinal pigment epithelium (RPE)/choroid complex to examine the expression of ADORA2A. The mRNA and protein expression of ADORA2A increased over time in fibrotic lesions, as demonstrated by quantitative reverse transcription polymerase chain reaction (RT-PCR) and Western blotting analysis (Fig. 1, D and E). In addition, by immunostaining of cross sections, we observed a notably increased expression of ADORA2A in the ACTA2-positive area (fig. S2), especially in samples from days 21 and 35. In contrast, the subretinal regions of noninjured mice were negative for ADORA2A staining. In human samples of wet AMD and in a mouse model of laser injury–induced CNV, respectively, compared with their controls, ADORA2A immunostaining was also more robust in the areas of the subretinal, outer/inner photoreceptor segments and the outer nuclear layer (Fig. 1B and fig. S2).

The genetic variation in the very low–density lipoprotein receptor (VLDLR) is linked to nAMD in humans (29). Mice lacking *Vldlr* (*Vldlr*$^{-/-}$) develop subretinal fibrosis even in 3 to 4 month olds and are therefore used as a genetic model for spontaneous nAMD (30, 31). We collected eyes and isolated RPE/choroid complex from *Vldlr*$^{-/-}$ and control mice to perform RT-PCR, Western blot, and immunostaining to examine the expression of ADORA2A in spontaneous subretinal fibrosis. The amounts of mRNA and protein for ADORA2A were increased in RPE/choroid complex from *Vldlr*$^{-/-}$ mice compared with those of control mice (Fig. 1, F and G). Furthermore, immunostaining showed higher ADORA2A expression

in the ACTA2-positive area of *Vldlr*$^{-/-}$ mice compared with the control mice (Fig. 1H). Collectively, these observations indicated an association of high ADORA2A expression with human AMD lesions and in two models for rodent subretinal fibrosis.

Global *Adora2a* deficiency improves subretinal fibrosis in *Vldlr*$^{-/-}$ and laser injury–induced CNV mouse models

To evaluate the impact of ADORA2A on subretinal fibrosis, we generated global inducible *Adora2a*-deficient mice (*Adora2a*$^{f/f}$; *Rosa26*$^{Cre/ERT2}$) by breeding *Adora2a*$^{flox/flox}$ with *Rosa26*$^{Cre/ERT2}$ mice to generate *Adora2a*^{iKO} mice after tamoxifen treatment (fig. S3, A and B). The mice of the littermate *Rosa26*$^{Cre/ERT2}$ (*Adora2a*^{WT}) were used as wild-type (WT) controls. Before the tamoxifen injection to delete *Adora2a*, regular retinal structure and blood flow were observed with spectral domain–optical coherence tomography (SD-OCT) and fluorescein angiography (FA) in these two groups of mice (fig. S3, C and D). In addition, there was no difference in visual acuity and photoreceptor function when the two groups were measured with the optomotor response (OMR) and pattern electroretinography (PERG) (fig. S3, E and F).

We deleted *Adora2a* in *Adora2a*$^{f/f}$;*Rosa26*$^{Cre/ERT2}$ mice by administering tamoxifen at 7 weeks of age, and 2 weeks later, we performed laser injury on these mice and analyzed the subretinal fibrosis at days 21 and 35 after injury. SD-O CT at day 21 after laser showed that the lesion size was smaller in *Adora2a*^{iKO} mice than in *Adora2a*^{WT} mice (fig. S4, A and B). There was no difference in visual acuity, as measured by OMR, or photoreceptor function, as measured by PERG, between the two groups of mice before laser injury (fig. S4, C and D). However, 21 days after laser injury, visual acuity was improved, and scotopic and photopic waves were enhanced in *Adora2a*^{iKO} mice compared with *Adora2a*^{WT} mice (fig. S4, C and D). Real-time PCR and Western blotting analysis of fibrotic markers in RPE/choroid of these mice showed that the amounts of mRNA and protein for ACTA2, SM22a, COL1, TGFβ2, and FN were lower in *Adora2a*^{iKO} mice than in *Adora2a*^{WT} mice (Fig. 2, A and B). Furthermore, the immunostaining of RPE/choroidal flat mounts with antibodies against COL1 and ACTA2 showed that subretinal fibrosis in *Adora2a*^{iKO} mice was markedly reduced at both days 21 and 35 compared with WT control mice (Fig. 2C). To corroborate these results in the *Vldlr*$^{-/-}$ mouse model for spontaneous subretinal fibrosis, we crossed *Adora2a*$^{f/f}$;*Rosa26*$^{Cre/ERT2}$ with *Vldlr*$^{-/-}$ mice to generate global *Adora2a*-deficient mice in *Vldlr*$^{-/-}$ background. As shown in Fig. 2 (D and E), *Vldlr*$^{-/-}$;*Adora2a*^{iKO} mice displayed less subretinal fibrosis than *Vldlr*$^{-/-}$;*Adora2a*^{WT} mice, as evidenced by decreased mRNA and protein for ACTA2, SM22a, COL1, and FN, as examined by real-time RT-PCR and Western blotting, as well as reduced Masson's trichrome staining and ACTA2 immunostaining (Fig. 2, F to H). These results demonstrated that *Adora2a* global deficiency improved laser-injured visual functions and attenuated the development of subretinal fibrosis in laser injury–induced CNV mice and *Vldlr*$^{-/-}$ mice.

Inducible global Adora2a deficiency attenuates laser injury–induced subretinal fibrosis

CNV in *Adora2a*^{iKO} mice at day 7 after laser injury was also decreased (fig. S5), indicating a possibility that suppressed subretinal fibrosis is secondary to reduced neovascularization. We therefore performed further studies to examine whether the inhibitory effect of *Adora2a*

deletion on subretinal fibrosis was independent of its antiangiogenic effect. As shown in Fig. 3A, the size of CNV and subretinal fibrosis at day 7 after laser injury was similar between *Rosa26*$^{Cre/ERT2}$ and *Adora2a*$^{f/f}$;*Rosa26*$^{Cre/ERT2}$ mice without tamoxifen treatment, indicating that the two types of mice respond similarly to laser injury. When tamoxifen treatment was performed at day 7 after laser, no difference in the size of CNV or subretinal fibrosis was observed at day 12 after laser (Fig. 3B), indicating that *Adora2a* deletion at the regression stage of CNV did not further accelerate regression of neovascularization and fibrosis. At day 35 after laser (tamoxifen injection from day 7 after laser), the size of subretinal fibrosis was reduced by 50% in *Adora2a*^{iKO} mice compared with the control mice (Fig. 3C), indicating that deletion of *Adora2a* at a late stage of post-angiogenesis reduced subretinal fibrosis in an antiangiogenic-independent manner.

EndMT plays a critical role in the development of subretinal fibrosis

EndMT has previously been shown to play a critical role in the pathogenesis of fibrosis (32, 33), but it has not been reported in subretinal fibrosis in vivo. To address this question, *Cdh5*^{Cre};*Rosa26-EYFP*$^{f/f}$ mice (fig. S6, A to E), whose ECs are fate-mapped with the Rosa26-stop-EYFP (enhanced yellow fluorescent protein) reporter, were subjected to laser-induced CNV. The expression of EC markers and mesenchymal cell markers in EYFP-positive cells at various time points was monitored to examine the long-term fate of ECs in subretinal fibrosis. As shown in Fig. 4A, 7 days after laser injury, EYFP-positive cells expressed the EC marker CD31 and mesenchymal cell marker ACTA2, suggesting that a subset of ECs was transdifferentiated into mesenchymal cells at the early-stage post-laser injury. Twenty-one days after laser injury, at the stage with dominant subretinal fibrotic lesions, the EC marker CD31 was weakly observed (Fig. 4B). However, a high amount of the mesenchymal cell marker ACTA2 in EYFP-positive cells was observed, indicating that these mesenchymal cells were transdifferentiated from ECs (Fig. 4, B and C). Flat-mount immunostaining results showed a similar phenotype (fig. S7, A to E). These findings demonstrated that EndMT played a role in the formation of subretinal fibrosis. We next examined ADORA2A expression in the retina samples collected from *Cdh5*^{Cre};*Rosa26-EYFP*$^{f/f}$ mice at days 7 and 21 after laser injury. As shown in fig. S8, we observed that EYFP-positive cells displayed ADORA2A expression at both days 7 and 21 after laser injury. These results indicated that ADORA2A was present in both ECs and EndMT cells.

EC Adora2a deficiency attenuates laser injury–induced subretinal fibrosis

To further investigate the role of ADORA2A in EndMT and subretinal fibrosis, we performed laser-induced CNV on endothelial-specific *Adora2a*-deficient mice (*Adora2a*$^{f/f}$;*Cdh5*$^{Cre/ERT2}$, *Adora2a*$^{\Delta iVEC}$). These mice were generated by breeding *Cdh5*$^{Cre/ERT2}$ mice with *Adora2a*$^{flox/flox}$ mice after tamoxifen treatment, and their littermate *Cdh5*$^{Cre/ERT2}$ mice (*Adora2a*^{WT}) were used as controls (fig. S9, A and B). As described above, tamoxifen treatment was performed at day 7 after laser on these mice. After euthanizing the mice at day 21 after injury, we collected RPE/choroidal samples for real-time PCR and Western blotting analysis of fibrotic markers (Fig. 5A). The results showed that the mRNA and protein ACTA2, SM22a, COL1, FN, and TGFβ2 were lower in *Adora2a*$^{\Delta iVEC}$ mice compared with *Adora2a*^{WT} mice (Fig. 5, B and C). Furthermore, immunostaining of RPE/choroidal flat mounts using antibodies against COL1 and ACTA2 showed that, at

days 21 and 35, the laser-induced collagen production in *Adora2a*$^{\Delta iVEC}$ mice was markedly reduced in contrast to a marked increase in subretinal fibrosis in control mice (Fig. 5, D and E). These data suggested that EC-specific deletion of *Adora2a* reduced the development of laser-induced subretinal fibrosis.

ADORA2A regulates EndMT in mouse models and human choroidal ECs

To investigate the regulatory role of ADORA2A in EndMT induction in vivo, we bred *Adora2a*$^{flox/flox}$ mice with *Cdh5*^{Cre};*Rosa26*-EYFP$^{f/f}$ mice to produce mice with *Adora2a* deficiency selectively in EYFP-ECs (*Adora2a*$^{f/f}$;*Cdh5*^{Cre};*Rosa26*-EYFP$^{f/f}$) and their controls (*Cdh5*^{Cre};*Rosa26*-EYFP$^{f/f}$). The mice underwent laser-induced CNV, and eyes were collected at day 21 after laser injury to determine whether EC *Adora2a* deficiency contributes to EndMT in vivo. Eye cross sections from these mice stained with antibodies against ACTA2 in EYFP-positive cells showed that ACTA2-positive area in the EYFP-positive area was much smaller in EC-specific *Adora2a* deletion mice than in control mice (Fig. 6A). These findings indicated that *Adora2a* was critical for EndMT induction in vivo.

To further examine the role of ADORA2A in regulating EndMT of choroidal ECs, we cultured human choroidal ECs (hCECs) and incubated them with human TGFβ2, a potent inducer of EndMT (fig. S9C). TGFβ2 enhanced the expression of ADORA2A and EndMT markers, including ACTA2, SM22α, COL1, and FN (Fig. 6B), indicating that ADORA2A may promote EndMT induction. Using a loss-of-function approach, *ADORA2A* expression on hCECs was knocked down with small interfering RNA (siRNA) of *ADORA2A* (si*ADORA2A*). Western blot analysis showed that *ADORA2A* knockdown (KD) decreased the amount of protein for ACTA2, SM22α, COL1, and FN and increased the amounts of protein for CDH5 in hCECs, especially in the cells treated with TGFβ2 (Fig. 6B). These loss-of-function studies were corroborated using a gain-of-function approach, in which we overexpressed *ADORA2A* in hCECs using an adenovirus vector. Ad-*ADORA2A* transfection elongated hCECs, increased the mRNA and protein expression of ACTA2, TAGLN (SM22α), COL1, and FN, and decreased CDH5 expression (Fig. 6, C to F) compared with transfection of control adenovirus Ad-*CTRL* in hCECs.

We next cultured mouse choroidal ECs (mCECs) of *Adora2a*$^{\Delta iVEC}$ or *Adora2a*^{WT} mice to examine the role of ADORA2A in EndMT induction (fig. S10A). In line with our hCECs studies, *Adora2a*^{WT} mCECs showed increased protein expression of ACTA2, SM22α, and COL1 and decreased CD31 in response to mouse TGFβ2 (mTGFβ2) compared with vehicle treatment (fig. S10B). In contrast, *Adora2a*$^{\Delta iVEC}$ mCECs expressed decreased protein expression of EndMT markers compared with *Adora2a*^{WT} mCECs in the presence of mTGFβ2 (fig. S10C). Collectively, these in vitro findings demonstrated the role of ADORA2A in regulating EndMT in both human and mouse choroidal ECs.

ADORA2A mediates the SDH-succinate signaling pathway to promote EndMT

To explore the mechanism whereby ADORA2A regulates EndMT, we examined the metabolomics profiles of hCECs transfected with si*ADORA2A* and treated with TGFβ2 by analyzing the cell extracts with liquid chromatography–tandem mass spectrometry (LC-MS/MS). TGFβ2 treatment changed the amounts of many metabolites in pathways

of glycolysis, pentose phosphate pathway, and hexosamine synthesis but not nucleic acid metabolic pathway. *ADORA2A* KD did not affect these metabolic pathways in hCECs (fig. S11, A to D). However, elevated succinate was observed in TGFβ2-treated hCECs, and this increased succinate was reduced by *ADORA2A* KD (Fig. 7A). On the basis of the changes in succinate abundance, we examined the expression of oxoglutarate dehydrogenase (OGDH) and succinate dehydrogenase (SDH) in TGFβ2-treated cells. TGFβ2 suppressed the expression of succinate dehydrogenase B (SDHB) but had no effect on OGDH expression, thus inducing succinate accumulation. *ADORA2A* KD rescued the decreased SDHB expression, thereby reducing succinate production (Fig. 7B). Overexpression of *ADORA2A* in hCECs down-regulated SDHB expression and did not change OGDH expression, resulting in increased succinate (Fig. 7, C and D). Consistent with these in vitro studies, Western blots with samples of RPE-choroidal complexes showed decreased expression of SDHB in laser-injured $Adora2a^{WT}$ mice compared with noninjured mice. The SDHB expression in laser-injured $Adora2a^{\Delta iVEC}$ was much higher than in laser-injured $Adora2a^{WT}$ mice (Fig. 7E). To further examine the association of SDHB and succinate with EndMT, we treated hCECs with exogenous succinate and detected EndMT-relevant molecules. As shown in Fig. 7F, exogenous succinate increased mesenchymal cell markers ACTA2 and SM22α, increased production of FN, and decreased EC marker CDH5. These results indicated that ADORA2A regulated SDHB, leading to subsequent changes in succinate production that contributed to EndMT induction in choroidal ECs.

Blockade of ADORA2A attenuates subretinal fibrosis in mice and EndMT in hCECs

To explore the therapeutic potential of targeting ADORA2A for the treatment of subretinal fibrosis, we first treated TGFβ2-stimulated hCECs with the ADORA2A pharmacologic antagonist KW6002 (0.1 μM) or vehicle for five consecutive days. As shown in fig. S12 (A and B), KW6002 treatment suppressed the amounts of mRNA and protein for ACTA2, TAGLN, and FN compared with vehicle treatment and increased EC marker CD31. To investigate the potential effect of KW6002 on myofibroblast activity, we also exposed hCECs to TGFβ2 for 3 days to induce EndMT. Then, we treated these cells with KW6002 (0.1 μM) or vehicle for an additional 4 days while maintaining TGFβ2 stimulation. Western blotting analysis revealed that KW6002 treatment decreased the amounts of protein for COL1 and FN compared with vehicle treatment (fig. S12C). These results demonstrated that the pharmacological inhibition of ADORA2A using KW6002 directly affected the myofibroblast activity associated with subretinal fibrosis. We next administered KW6002 (10 mg/kg) by daily intraperitoneal injections to C57BL/6 mice beginning on day 7 after laser-induced CNV until 35 days after laser injury. The RPE/choroid complexes of these mice were immunostained with COL1 and ACTA2 antibodies and showed a much smaller size of the fibrotic area in samples from mice treated with KW6002 than those treated with vehicle (Fig. 8A). In addition to intraperitoneal injections of KW6002, we also administrated mice with KW6002 through oral gavage. We observed the same inhibitory effect of this antagonist on the formation of subretinal fibrosis (Fig. 8B). We also treated $Vldlr^{-/-}$ mice at 8 weeks old with KW6002 or vehicle daily intraperitoneal injections for 8 weeks (fig. S13, A and B). The RPE/choroid complexes were analyzed by quantitative RT-PCR, Western blotting, and histological analysis. The amounts of mRNA for *Col1a1*, *Acta2*, *Tagln*, *Fn*, *Ctgf*, and *Fgf2* were lower in $Vldlr^{-/-}$ mice treated with KW6002 compared

with those of mice with vehicle. In addition, the amounts of protein for COL1, ACTA2, SM22α, and FN were decreased in *Vldlr*$^{-/-}$ mice treated with KW6002 compared with mice treated with vehicle (Fig. 8, C and D). Staining with hematoxylin and eosin (H&E), Masson's trichrome, and ACTA2 anti-body showed decreased areas of fibrosis in *Vldlr*$^{-/-}$ mice treated with KW6002 (Fig. 8, E to G). *Cdh5*^{Cre};*Rosa26-EYFP*$^{f/f}$ mice subjected to laser injury were also treated with KW6002 by daily intraperitoneal injections (Fig. 8H). Eyes from these mice were examined, and the area of EYFP-ACTA2 double staining was smaller in mice treated with KW6002 than in mice treated with vehicle (Fig. 8H). These observations demonstrated that pharmacologic inhibition of ADORA2A with KW6002 effectively reduced the development of subretinal fibrosis by suppressing EndMT.

DISCUSSION

In a genome-wide study, ADORA2A was identified as an important determinant of human vascular disease (34). Its role in ocular vascular disorders has been an active area of research. The high incidence of PDR in a cohort of patients with type 1 diabetes has been associated with the single-nucleotide polymorphism type of ADORA2A that results in its high expression (23, 35). Increased expression of ADORA2A in retinal ECs boosted glycolysis and increased tip cell migration and stalk cell proliferation, enhancing angiogenesis (23). Reanalysis of microarray gene expression data of retinal FVMs from patients with PDR has demonstrated an association of ADORA2A with ocular fibrosis (26). The current study further demonstrates a causal role of ADORA2A in the development of ocular fibrosis, especially the formation of subretinal fibrosis (fig. S14).

Specifically, we focused on the role of endothelial ADORA2A in the development of subretinal fibrosis in patients with nAMD, a disease characterized by pathological angiogenesis. Anti–vascular endothelial growth factor (VEGF) therapy is the primary treatment for nAMD. However, despite monthly treatment, approximately one-fourth of nAMD eyes still develop subretinal fibrosis (36). Multiple factors contribute to this outcome. Nevertheless, a recent study has shown that anti-VEGF therapy promotes EndMT, thereby increasing the incidence of subretinal fibrosis (14). This finding underscores the importance of investigating the cause of EndMT and subretinal fibrosis in nAMD eyes. Using a combination of human and rodent models with genetic and pharmacologic approaches, we provide evidence that ADORA2A in choroidal ECs is essential for EndMT in CNV lesions and, in turn, the development of subretinal fibrosis.

In addition to EndMT, suppressing subretinal fibrosis after inactivation of endothelial ADORA2A is attributed to many other mechanisms. We have shown that deleting/blocking *Adora2a* can inhibit pathological angiogenesis in a mouse oxygen-induced retinopathy model. In the laser-induced CNV model, small CNV lesions are also observed in mice with deletion/blockade of *Adora2a*. ADORA2A is highly expressed in αSMA/ACTA2-positive cells, which indicates that fully differentiated myofibroblasts express ADORA2A/Adora2a. Suppression of fibroblast ADORA2A is able to inhibit skin scar formation (37). ADORA2A suppression of choroid EC–transited myofibroblasts with KW6002 inhibits their fibrotic activity. Thus, suppression of choroidal endothelial proliferation and fibrotic activity of

myofibroblasts are also underlying mechanisms for suppressed subretinal fibrosis in mice lacking endothelial *Adora2a*.

The effect of ADORA2A-mediated EndMT appears to involve distinct metabolic reprogramming. Consistent with a previous study on the role of TGFβ1 in metabolic changes (38), treatment with TGFβ2 increased succinate, a metabolite in the tricarboxylic acid (TCA) that plays a role in the development of inflammation, metabolic disorders, and cancers (39, 40). It has been demonstrated that succinate is an essential mediator in the development of pulmonary fibrosis (41). Succinate can induce mesenchymal transition of choroidal ECs. KD of *ADORA2A* reduced the elevated succinate in TGFβ2-treated choroidal ECs, whereas up-regulation of *ADORA2A* enhanced succinate production. This was accompanied by the dynamic change of SDHB, a subunit of SDH causing succinate accumulation under various pathological conditions (42). These results suggested the involvement of the ADORA2A-S DH-succinate axis in the development of subretinal fibrosis. Furthermore, our study and others have characterized the role of hypoxia-inducible factor 1α (HIF1α) inflammasome in endothelial angiogenesis and myeloid inflammation induced by ADORA2A (23, 43). Many studies have shown that succinate accumulation stabilizes HIF (44, 45). Therefore, we speculate that other pathways, such as HIF and inflammasomes, may also be directly or indirectly involved in the anti-fibrotic effect of *ADORA2A* KD in subretinal fibrosis.

This study has limitations. The study specifically focused on the role of endothelial ADORA2A in subretinal fibrosis. However, the impact of ADORA2A originating from other cell types cannot be dismissed, because it may also play a crucial role in subretinal fibrosis. Myofibroblasts involved in subretinal fibrosis can also arise from RPE cells and myeloid cells (9, 10, 12). For instance, during AMD, RPE cells exhibit degeneration, leading to the loss of their characteristic epithelial morphology and function. These cells transform into mesenchymal cells through a process known as epithelial-mesenchymal transition (46–49). Furthermore, macrophages exist in both human CNV lesions (50) and mouse experimental CNV (51, 52). These macrophages undergo a process called an MMT, contributing to the formation of subretinal fibrosis (12). ADORA2A is present in both RPE and myeloid cells (43, 53). The selective ADORA2A antagonists have been shown to prevent microglia-mediated neuroinflammation, thereby protecting retinal ganglion cells, RPE cells, and photoreceptors in in vitro and in vivo studies (54, 55). In addition to cells directly involved in subretinal fibrosis, cells of outer/inner photoreceptor segments and the outer nuclear layer also display increased expression of ADORA2A in human samples of wet AMD and in a mouse model of laser injury–induced CNV compared with their controls. The association between the photoreceptors and AMD has been noted in the literature (56, 57). Therefore, the up-regulated ADORA2A in these non-subretinal cells may indirectly participate in the subretinal fibrosis. Hence, the observed suppression of subretinal fibrosis in global inducible *Adora2a*-deficient mice and mice treated with KW6002 could also be due, in part, to the inactivity of ADORA2A in many types of cells other than choroidal ECs. In future studies, consideration should be given to investigating the impact of ADORA2A on the abovementioned cells in subretinal fibrosis.

Suppressed subretinal fibrosis in mice after ADORA2A blockade shows the translational nature of ADORA2A antagonists. Over the past decades, various types of ADORA2A inhibitors have been developed to aim at treating different disorders, and some of them have shown a high specificity for ADORA2A compared with other adenosine receptors (58, 59). Among these inhibitors, KW6002 has been extensively studied and received approval from the US Food and Drug Administration in 2019 to treat Parkinson's disease. One advantage of KW6002 is its oral administration route, which distinguishes it from anti-VEGF reagents that require local administration through intravitreal or subretinal injections and often cause side effects (60). Given these findings, investigating the potential of ADORA2A blockade in patients with nAMD and subretinal fibrosis emerges as a practical and feasible approach.

MATERIALS AND METHODS

Study design

The major goal of this study was to investigate the impact of ADORA2A on the development of subretinal fibrosis, as well as to determine whether inhibiting or blocking this molecule could reduce the size of subretinal fibrotic lesions. To address this, in vivo experiments for loss-of-function studies were performed in a model of laser injury–induced mouse CNV and *Vldlr*$^{-/-}$ mice with mice in the absence of global or endothelial-specific deletion of *Adora2a*. Pharmacologic inhibition of ADORA2A with KW6002 was also conducted in these two mouse models. Endothelial lineage tracing mice were generated to investigate the further underlying mechanism. In addition, choroidal ECs from these mice were isolated, and hCECs were cultured for in vitro mechanistic study. Each experimental group consisted of a minimum of six mice to ensure a robust demonstration of differences in subretinal fibrosis phenotypes and the expression of relevant genes. The minimum animal numbers and sample sizes required to achieve statistical significance were determined by power analysis and prior experience from literature. The assignment of mice to control and treatment groups was done randomly. Data analyses for in vivo subretinal fibrosis phenotypes were performed in a blinded manner. The control and treatment groups, sample sizes, and the specific statistical tests used for each experiment are outlined in the figure legends. All original data can be found in data file S1.

Statistical analysis

All studies were designed to generate groups of optimal size using randomization. Researchers were blinded to the evaluation of experimental outcomes and analysis of the raw data. Some results were normalized to the control to avoid unwanted sources of variation. Statistical analysis was performed using GraphPad Prism software (version 8.0, RRID: SCR_000306), and data are presented as means ± SEM. No outliers were removed from the data. Statistical analysis was only undertaken for studies where each group size was at least $n = 5$. N represents the number of studied animals (in vivo) or independent values (in vitro), and statistical analysis was performed using these separate values. Data distribution was assessed by the Shapiro-Wilk test for normality, and the F test or Brown-Forsythe test was performed to test the equality of variance. For comparisons of two groups, unpaired two-t ailed Student's t test (when the variances were equal) or unpaired two-t ailed Student's t test with Welch's correction (when variances were unequal) was performed when normal

distribution was satisfied. Otherwise, nonparametric Mann-Whitney tests were performed for the datasets where normal distribution was not satisfied. For multiple groups, Brown-Forsythe test was used to test the homogeneity of variance. Differences among multiple groups were assessed by one-way analysis of variance (ANOVA) followed by a Bonferroni post hoc analysis or two-way ANOVA followed by Tukey post hoc test (for experiments with two factors) for the datasets satisfied by the Brown-Forsythe test, otherwise by one-way ANOVA and Welch's ANOVA test with Dunnett's T3 multiple comparisons. $P < 0.05$ was considered significant. Tests used for statistical analysis for each experiment are specified in table S7.

Supplementary Material

Refer to Web version on PubMed Central for supplementary material.

Acknowledgments

Funding:

This work was supported by grants from the National Institutes of Health (R01 EY030500, R01 EY033369, and R01 EY033737 to R.B.C. and Y.H.), National Eye Institute K99 award (1K99EY034577-01A1 to Q.Y.), and P30EY031631.

Data and materials availability:

All data associated with this study are present in the paper or the Supplementary Materials. The microarray results are available in the NCBI's Gene Expression Omnibus (GEO) database (accession number, GSE60436). The original metabolomics data have been uploaded to Dryad with a unique digital object identifier (DOI): doi:10.5061/dryad.hx3ffbgmv, or by URL: https://datadryad.org/stash/share/miRgmqSGb1b4tD3XqKUFVdX3V7-fkxrW8YTbZpL4xPQ. New mouse strains will be available via material transfer agreement upon request to the corresponding author.

REFERENCES AND NOTES.

1. Jager RD, Mieler WF, Miller JW, Age-related macular degeneration. N. Engl. J. Med. 358, 2606–2617 (2008). [PubMed: 18550876]
2. Ambati J, Fowler BJ, Mechanisms of age-related macular degeneration. Neuron 75, 26–39 (2012). [PubMed: 22794258]
3. Jonas JB, Global prevalence of age-related macular degeneration. Lancet Glob. Health 2, e65–e66 (2014). [PubMed: 25104656]
4. Wong WL, Su X, Li X, Cheung CM, Klein R, Cheng CY, Wong TY, Global prevalence of age-related macular degeneration and disease burden projection for 2020 and 2040: A systematic review and meta-analysis. Lancet Glob. Health 2, e106–e116 (2014). [PubMed: 25104651]
5. Ryan SJ, The development of an experimental model of subretinal neovascularization in disciform macular degeneration. Trans. Am. Ophthalmol. Soc. 77, 707–745 (1979). [PubMed: 94717]
6. Stevens TS, Bressler NM, Maguire MG, Bressler SB, Fine SL, Alexander J, Phillips DA, Margherio RR, Murphy PL, Schachat AP, Occult choroidal neovascularization in age-related macular degeneration. A natural history study. Arch. Ophthalmol. 115, 345–350 (1997). [PubMed: 9076206]
7. Viola F, Massacesi A, Orzalesi N, Ratiglia R, Staurenghi G, Retinal angiomatous proliferation: Natural history and progression of visual loss. Retina 29, 732–739 (2009). [PubMed: 19516115]

8. Lim LS, Mitchell P, Seddon JM, Holz FG, Wong TY, Age-related macular degeneration. Lancet 379, 1728–1738 (2012). [PubMed: 22559899]
9. Ishikawa K, Kannan R, Hinton DR, Molecular mechanisms of subretinal fibrosis in age-related macular degeneration. Exp. Eye Res. 142, 19–25 (2016). [PubMed: 25773985]
10. Shu DY, Lovicu FJ, Myofibroblast transdifferentiation: The dark force in ocular wound healing and fibrosis. Prog. Retin. Eye Res. 60, 44–65 (2017). [PubMed: 28807717]
11. Shu DY, Butcher E, Saint-Geniez M, EMT and EndMT: Emerging roles in age-related macular degeneration. Int. J. Mol. Sci. 21, 4271 (2020). [PubMed: 32560057]
12. Little K, Llorián-Salvador M, Tang M, Du X, Marry S, Chen M, Xu H, Macrophage to myofibroblast transition contributes to subretinal fibrosis secondary to neovascular age-related macular degeneration. J. Neuroinflammation 17, 355 (2020). [PubMed: 33239022]
13. Abu El-Asrar AM, De Hertogh G, van den Eynde K, Alam K, Van Raemdonck K, Opdenakker G, Van Damme J, Geboes K, Struyf S, Myofibroblasts in proliferative diabetic retinopathy can originate from infiltrating fibrocytes and through endothelial-to-mesenchymal transition (EndoMT). Exp. Eye Res. 132, 179–189 (2015). [PubMed: 25637870]
14. Rossato FA, Su Y, Mackey A, Ng YSE, Fibrotic changes and endothelial-to-mesenchymal transition promoted by VEGFR2 antagonism alter the therapeutic effects of VEGFA pathway blockage in a mouse model of choroidal neovascularization. Cell 9, 2057 (2020).
15. Wang H, Ramshekar A, Kunz E, Hartnett ME, 7-ketocholesterol induces endothelial-mesenchymal transition and promotes fibrosis: Implications in neovascular age-related macular degeneration and treatment. Angiogenesis 24, 583–595 (2021). [PubMed: 33646466]
16. Kovacic JC, Mercader N, Torres M, Boehm M, Fuster V, Epithelial-to-mesenchymal and endothelial-to-mesenchymal transition: From cardiovascular development to disease. Circulation 125, 1795–1808 (2012). [PubMed: 22492947]
17. Chen JF, Eltzschig HK, Fredholm BB, Adenosine receptors as drug targets—What are the challenges? Nat. Rev. Drug Discov. 12, 265–286 (2013). [PubMed: 23535933]
18. Fredholm BB, AP IJ, Jacobson KA, Linden J, Müller CE, International union of basic and clinical pharmacology. LXXXI. Nomenclature and classification of adenosine receptors—An update. Pharmacol. Rev. 63, 1–34 (2011). [PubMed: 21303899]
19. Fredholm BB, Arslan G, Halldner L, Kull B, Schulte G, Wasserman W, Structure and function of adenosine receptors and their genes. Naunyn Schmiedebergs Arch. Pharmacol. 362, 364–374 (2000). [PubMed: 11111830]
20. Kull B, Svenningsson P, Fredholm BB, Adenosine A(2A) receptors are colocalized with and activate g(olf) in rat striatum. Mol. Pharmacol. 58, 771–777 (2000). [PubMed: 10999947]
21. Corvol JC, Studler JM, Schonn JS, Girault JA, Hervé D, Galpha(olf) is necessary for coupling D1 and A2a receptors to adenylyl cyclase in the striatum. J. Neurochem. 76, 1585–1588 (2001). [PubMed: 11238742]
22. Eltzschig HK, Sitkovsky MV, Robson SC, Purinergic signaling during inflammation. N. Engl. J. Med. 367, 2322–2333 (2012). [PubMed: 23234515]
23. Liu Z, Yan S, Wang J, Xu Y, Wang Y, Zhang S, Xu X, Yang Q, Zeng X, Zhou Y, Gu X, Lu S, Fu Z, Fulton DJ, Weintraub NL, Caldwell RB, Zhang W, Wu C, Liu X-L, Chen J-F, Ahmad A, Kaddour-Djebbar I, Al-Shabrawey M, Li Q, Jiang X, Sun Y, Sodhi A, Smith L, Hong M, Huo Y, Endothelial adenosine A2a receptor-mediated glycolysis is essential for pathological retinal angiogenesis. Nat. Commun. 8, 584 (2017). [PubMed: 28928465]
24. Zhang S, Zhou R, Li B, Li H, Wang Y, Gu X, Tang L, Wang C, Zhong D, Ge Y, Huo Y, Lin J, Liu XL, Chen JF, Caffeine preferentially protects against oxygen-induced retinopathy. FASEB J. 31, 3334–3348 (2017). [PubMed: 28420694]
25. Chen JF, Zhang S, Zhou R, Lin Z, Cai X, Lin J, Huo Y, Liu X, Adenosine receptors and caffeine in retinopathy of prematurity. Mol. Aspects Med. 55, 118–125 (2017). [PubMed: 28088487]
26. Ishikawa K, Yoshida S, Kobayashi Y, Zhou Y, Nakama T, Nakao S, Sassa Y, Oshima Y, Niiro H, Akashi K, Kono T, Ishibashi T, Microarray analysis of gene expression in fibrovascular membranes excised from patients with proliferative diabetic retinopathy. Invest. Ophthalmol. Vis. Sci. 56, 932–946 (2015). [PubMed: 25604687]

27. Ishikawa K, Sreekumar PG, Spee C, Nazari H, Zhu D, Kannan R, Hinton DR, αB-Crystallin regulates subretinal bibrosis by modulation of epithelial-mesenchymal transition. Am. J. Pathol. 186, 859–873 (2016). [PubMed: 26878210]
28. Little K, Llorián-Salvador M, Tang M, Du X, O'Shaughnessy Ó, McIlwaine G, Chen M, Xu H, A two-stage laser-induced mouse model of subretinal fibrosis secondary to choroidal neovascularization. Transl. Vis. Sci. Technol. 9, 3 (2020).
29. Haines JL, Schnetz-Boutaud N, Schmidt S, Scott WK, Agarwal A, Postel EA, Olson L, Kenealy SJ, Hauser M, Gilbert JR, Pericak-Vance MA, Functional candidate genes in age-related macular degeneration: Significant association with VEGF, VLDLR, and LRP6. Invest. Ophthalmol. Vis. Sci. 47, 329–335 (2006). [PubMed: 16384981]
30. Heckenlively JR, Hawes NL, Friedlander M, Nusinowitz S, Hurd R, Davisson M, Chang B, Mouse model of subretinal neovascularization with choroidal anastomosis. Retina 23, 518–522 (2003). [PubMed: 12972764]
31. Hu W, Jiang A, Liang J, Meng H, Chang B, Gao H, Qiao X, Expression of VLDLR in the retina and evolution of subretinal neovascularization in the knockout mouse model's retinal angiomatous proliferation. Invest. Ophthalmol. Vis. Sci. 49, 407–415 (2008). [PubMed: 18172119]
32. Piera-Velazquez S, Jimenez SA, Endothelial to mesenchymal transition: Role in physiology and in the pathogenesis of human diseases. Physiol. Rev. 99, 1281–1324 (2019). [PubMed: 30864875]
33. Jackson AO, Zhang J, Jiang Z, Yin K, Endothelial-to-mesenchymal transition: A novel therapeutic target for cardiovascular diseases. Trends Cardiovasc. Med. 27, 383–393 (2017). [PubMed: 28438397]
34. Nikpay M, Goel A, Won HH, Hall LM, Willenborg C, Kanoni S, Saleheen D, Kyriakou T, Nelson CP, Hopewell JC, Webb TR, Zeng L, Dehghan A, Alver M, Armasu SM, Auro K, Bjonnes A, Chasman DI, Chen S, Ford I, Franceschini N, Gieger C, Grace C, Gustafsson S, Huang J, Hwang SJ, Kim YK, Kleber ME, Lau KW, Lu X, Lu Y, Lyytikäinen LP, Mihailov E, Morrison AC, Pervjakova N, Qu L, Rose LM, Salfati E, Saxena R, Scholz M, Smith AV, Tikkanen E, Uitterlinden A, Yang X, Zhang W, Zhao W, de Andrade M, de Vries PS, van Zuydam NR, Anand SS, Bertram L, Beutner F, Dedoussis G, Frossard P, Gauguier D, Goodall AH, Gottesman O, Haber M, Han BG, Huang J, Jalilzadeh S, Kessler T, König IR, Lannfelt L, Lieb W, Lind L, Lindgren CM, Lokki ML, Magnusson PK, Mallick NH, Mehra N, Meitinger T, Memon FU, Morris AP, Nieminen MS, Pedersen NL, Peters A, Rallidis LS, Rasheed A, Samuel M, Shah SH, Sinisalo J, Stirrups KE, Trompet S, Wang L, Zaman KS, Ardissino D, Boerwinkle E, Borecki IB, Bottinger EP, Buring JE, Chambers JC, Collins R, Cupples LA, Danesh J, Demuth I, Elosua R, Epstein SE, Esko T, Feitosa MF, Franco OH, Franzosi MG, Granger CB, Gu D, Gudnason V, Hall AS, Hamsten A, Harris TB, Hazen SL, Hengstenberg C, Hofman A, Ingelsson E, Iribarren C, Jukema JW, Karhunen PJ, Kim BJ, Kooner JS, Kullo IJ, Lehtimäki T, Loos RJF, Melander O, Metspalu A, März W, Palmer CN, Perola M, Quertermous T, Rader DJ, Ridker PM, Ripatti S, Roberts R, Salomaa V, Sanghera DK, Schwartz SM, Seedorf U, Stewart AF, Stott DJ, Thiery J, Zalloua PA, O'Donnell CJ, Reilly MP, Assimes TL, Thompson JR, Erdmann J, Clarke R, Watkins H, Kathiresan S, McPherson R, Deloukas P, Schunkert H, Samani NJ, Farrall M, A comprehensive 1,000 genomes-based genome-wide association meta-analysis of coronary artery disease. Nat. Genet. 47, 1121–1130 (2015). [PubMed: 26343387]
35. Charles BA, Conley YP, Chen G, Miller RG, Dorman JS, Gorin MB, Ferrell RE, Sereika SM, Rotimi CN, Orchard TJ, Variants of the adenosine A(2A) receptor gene are protective against proliferative diabetic retinopathy in patients with type 1 diabetes. Ophthalmic Res. 46, 1–8 (2011). [PubMed: 21088442]
36. Daniel E, Toth CA, Grunwald JE, Jaffe GJ, Martin DF, Fine SL, Huang J, Ying GS, Hagstrom SA, Winter K, Maguire MG, Risk of scar in the comparison of age-related macular degeneration treatments trials. Ophthalmology 121, 656–666 (2014). [PubMed: 24314839]
37. Perez-Aso M, Chiriboga L, Cronstein BN, Pharmacological blockade of adenosine A2A receptors diminishes scarring. FASEB J. 26, 4254–4263 (2012). [PubMed: 22767233]
38. Xu Y, Li Y, Chen X, Xiang F, Deng Y, Li Z, Wei D, TGF-β protects osteosarcoma cells from chemotherapeutic cytotoxicity in a SDH/HIF1α dependent manner. BMC Cancer 21, 1200 (2021). [PubMed: 34763667]

39. Osuna-Prieto FJ, Martinez-Tellez B, Ortiz-Alvarez L, Di X, Jurado-Fasoli L, Xu H, Ceperuelo-Mallafré V, Núñez-Roa C, Kohler I, Segura-Carretero A, García-Lario JV, Gil A, Aguilera CM, Llamas-Elvira JM, Rensen PCN, Vendrell J, Ruiz JR, Fernández-Veledo S, Elevated plasma succinate levels are linked to higher cardiovascular disease risk factors in young adults. Cardiovasc. Diabetol. 20, 151 (2021). [PubMed: 34315463]
40. Terra X, Ceperuelo-Mallafré V, Merma C, Benaiges E, Bosch R, Castillo P, Flores JC, León X, Valduvieco I, Basté N, Cámara M, Lejeune M, Gumà J, Vendrell J, Vilaseca I, Fernández-Veledo S, Avilés-Jurado FX, Succinate pathway in head and neck squamous cell carcinoma: Potential as a diagnostic and prognostic marker. Cancer 13, 1653 (2021).
41. Xie N, Tan Z, Banerjee S, Cui H, Ge J, Liu RM, Bernard K, Thannickal VJ, Liu G, Glycolytic reprogramming in myofibroblast differentiation and lung fibrosis. Am. J. Respir. Crit. Care Med. 192, 1462–1474 (2015). [PubMed: 26284610]
42. Hobert JA, Mester JL, Moline J, Eng C, Elevated plasma succinate in PTEN, SDHB, and SDHD mutation-positive individuals. GIM 14, 616–619 (2012).
43. Ouyang X, Ghani A, Malik A, Wilder T, Colegio OR, Flavell RA, Cronstein BN, Mehal WZ, Adenosine is required for sustained inflammasome activation via the A_2A receptor and the HIF-1α pathway. Nat. Commun. 4, 2909 (2013). [PubMed: 24352507]
44. Selak MA, Armour SM, MacKenzie ED, Boulahbel H, Watson DG, Mansfield KD, Pan Y, Simon MC, Thompson CB, Gottlieb E, Succinate links TCA cycle dysfunction to oncogenesis by inhibiting HIF-alpha prolyl hydroxylase. Cancer Cell 7, 77–85 (2005). [PubMed: 15652751]
45. Guzy RD, Sharma B, Bell E, Chandel NS, Schumacker PT, Loss of the SdhB, but not the SdhA, subunit of complex II triggers reactive oxygen species-dependent hypoxia-inducible factor activation and tumorigenesis. Mol. Cell. Biol. 28, 718–731 (2008). [PubMed: 17967865]
46. Sarks JP, Sarks SH, Killingsworth MC, Evolution of geographic atrophy of the retinal pigment epithelium. Eye 2, 552–577 (1988). [PubMed: 2476333]
47. Guidry C, Medeiros NE, Curcio CA, Phenotypic variation of retinal pigment epithelium in age-related macular degeneration. Invest. Ophthalmol. Vis. Sci. 43, 267–273 (2002). [PubMed: 11773041]
48. Zanzottera EC, Messinger JD, Ach T, Smith RT, Curcio CA, Subducted and melanotic cells in advanced age-related macular degeneration are derived from retinal pigment epithelium. Invest. Ophthalmol. Vis. Sci. 56, 3269–3278 (2015). [PubMed: 26024109]
49. Lopez PF, Sippy BD, Lambert HM, Thach AB, Hinton DR, Transdifferentiated retinal pigment epithelial cells are immunoreactive for vascular endothelial growth factor in surgically excised age-related macular degeneration-related choroidal neovascular membranes. Invest. Ophthalmol. Vis. Sci. 37, 855–868 (1996). [PubMed: 8603870]
50. Grossniklaus HE, Ling JX, Wallace TM, Dithmar S, Lawson DH, Cohen C, Elner VM, Elner SG, Sternberg P Jr., Macrophage and retinal pigment epithelium expression of angiogenic cytokines in choroidal neovascularization. Mol. Vis. 8, 119–126 (2002). [PubMed: 11979237]
51. Espinosa-Heidmann DG, Caicedo A, Hernandez EP, Csaky KG, Cousins SW, Bone marrow-derived progenitor cells contribute to experimental choroidal neovascularization. Invest. Ophthalmol. Vis. Sci. 44, 4914–4919 (2003). [PubMed: 14578417]
52. Espinosa-Heidmann DG, Reinoso MA, Pina Y, Csaky KG, Caicedo A, Cousins SW, Quantitative enumeration of vascular smooth muscle cells and endothelial cells derived from bone marrow precursors in experimental choroidal neovascularization. Exp. Eye Res. 80, 369–378 (2005). [PubMed: 15721619]
53. Goebel CP, Song YS, Zaitoun IS, Wang S, Potter HAD, Sorenson CM, Sheibani N, Adenosine receptors expression in human retina and choroid with age-related macular degeneration. J. Ophthalmic Vis. Res. 18, 51–59 (2023). [PubMed: 36937188]
54. Madeira MH, Boia R, Elvas F, Martins T, Cunha RA, Ambrósio AF, Santiago AR, Selective A2A receptor antagonist prevents microglia-mediated neuroinflammation and protects retinal ganglion cells from high intraocular pressure-induced transient ischemic injury. Transl. Res. 169, 112–128 (2016). [PubMed: 26685039]

55. Madeira MH, Rashid K, Ambrósio AF, Santiago AR, Langmann T, Blockade of microglial adenosine A2A receptor impacts inflammatory mechanisms, reduces ARPE-19 cell dysfunction and prevents photoreceptor loss in vitro. Sci. Rep. 8, 2272 (2018). [PubMed: 29396515]
56. Zekavat SM, Sekimitsu S, Ye Y, Raghu V, Zhao H, Elze T, Segrè AV, Wiggs JL, Natarajan P, Del Priore L, Zebardast N, Wang JC, Photoreceptor layer thinning is an early biomarker for age-related macular degeneration: Epidemiologic and genetic evidence from UK Biobank OCT Data. Ophthalmology 129, 694–707 (2022). [PubMed: 35149155]
57. Joyal JS, Sun Y, Gantner ML, Shao Z, Evans LP, Saba N, Fredrick T, Burnim S, Kim JS, Patel G, Juan AM, Hurst CG, Hatton CJ, Cui Z, Pierce KA, Bherer P, Aguilar E, Powner MB, Vevis K, Boisvert M, Fu Z, Levy E, Fruttiger M, Packard A, Rezende FA, Maranda B, Sapieha P, Chen J, Friedlander M, Clish CB, Smith LE, Retinal lipid and glucose metabolism dictates angiogenesis through the lipid sensor Ffar1. Nat. Med. 22, 439–445 (2016). [PubMed: 26974308]
58. Müller CE, Jacobson KA, Recent developments in adenosine receptor ligands and their potential as novel drugs. Biochim. Biophys. Acta 1808, 1290–1308 (2011). [PubMed: 21185259]
59. Jenner P, An overview of adenosine A2A receptor antagonists in Parkinson's disease. Int. Rev. Neurobiol. 119, 71–86 (2014). [PubMed: 25175961]
60. Falavarjani KG, Nguyen QD, Adverse events and complications associated with intravitreal injection of anti-VEGF agents: A review of literature. Eye (Lond.) 27, 787–794 (2013). [PubMed: 23722722]
61. Wang Y, Nakayama M, Pitulescu ME, Schmidt TS, Bochenek ML, Sakakibara A, Adams S, Davy A, Deutsch U, Lüthi U, Barberis A, Benjamin LE, Mäkinen T, Nobes CD, Adams RH, Ephrin-B2 controls VEGF-induced angiogenesis and lymphangiogenesis. Nature 465, 483–486 (2010). [PubMed: 20445537]
62. Ma Q, Yang Q, Xu J, Zhang X, Kim D, Liu Z, Da Q, Mao X, Zhou Y, Cai Y, Pareek V, Kim HW, Wu G, Dong Z, Song W-L, Gan L, Zhang C, Hong M, Benkovic SJ, Weintraub NL, Fulton D, Asara JM, Ben-Sahra I, Huo Y, ATIC-associated de novo purine synthesis is critically involved in proliferative arterial disease. Circulation 146, 1444–1460 (2022). [PubMed: 36073366]
63. Zhou Y, Zeng X, Li G, Yang Q, Xu J, Zhang M, Mao X, Cao Y, Wang L, Xu Y, Wang Y, Zhang Y, Xu Z, Wu C, Chen J-F, Hoda MN, Liu Z, Hong M, Huo Y, Inactivation of endothelial adenosine A2A receptors protects mice from cerebral ischaemia-induced brain injury. Br. J. Pharmacol. 176, 2250–2263 (2019). [PubMed: 30931525]
64. Chen J-F, Xu K, Petzer JP, Staal R, Xu Y-H, Beilstein M, Sonsalla PK, Castagnoli K, Castagnoli N, Schwarzschild MA, Neuroprotection by caffeine and A2A adenosine receptor inactivation in a model of Parkinson's disease. J. Neurosci. 21, RC143 (2001).
65. Zhou R, Zhang S, Gu X, Ge Y, Zhong D, Zhou Y, Tang L, Liu X-L, Chen J-F, Adenosine A2A receptor antagonists act at the hyperoxic phase to confer protection against retinopathy. Mol. Med. 24, 41 (2018). [PubMed: 30134834]
66. Liu Z, Mao X, Yang Q, Zhang X, Xu J, Ma Q, Zhou Y, Da Q, Cai Y, Sopeyin A, Dong Z, Hong M, Caldwell RB, Sodhi A, Huo Y, Suppression of myeloid PFKFB3-driven glycolysis protects mice from choroidal neovascularization. Br. J. Pharmacol. 179, 5109–5131 (2022). [PubMed: 35830274]
67. Gong Y, Li J, Sun Y, Fu Z, Liu CH, Evans L, Tian K, Saba N, Fredrick T, Morss P, Chen J, Smith LE, Optimization of an image-guided laser-induced choroidal neovascularization model in mice. PLOS ONE 10, e0132643 (2015).
68. Shao Z, Friedlander M, Hurst CG, Cui Z, Pei DT, Evans LP, Juan AM, Tahiri H, Duhamel F, Chen J, Sapieha P, Chemtob S, Joyal JS, Smith LE, Choroid sprouting assay: An ex vivo model of microvascular angiogenesis. PLOS ONE 8, e69552 (2013).
69. Yang Q, Xu J, Ma Q, Liu Z, Sudhahar V, Cao Y, Wang L, Zeng X, Zhou Y, Zhang M, Xu Y, Wang Y, Weintraub NL, Zhang C, Fukai T, Wu C, Huang L, Han Z, Wang T, Fulton DJ, Hong M, Huo Y, PRKAA1/AMPKα1-driven glycolysis in endothelial cells exposed to disturbed flow protects against atherosclerosis. Nat. Commun. 9, 4667 (2018). [PubMed: 30405100]
70. Yang Q, Ma Q, Xu J, Liu Z, Mao X, Zhou Y, Cai Y, Da Q, Hong M, Weintraub NL, Fulton DJ, Belin de Chantemèle EJ, Huo Y, Endothelial AMPKα1/PRKAA1 exacerbates inflammation in HFD-fed mice. Br. J. Pharmacol. 179, 1661–1678 (2022). [PubMed: 34796475]

71. Yang Q, Cai Y, Ma Q, Xiong A, Xu P, Zhang Z, Xu J, Zhou Y, Liu Z, Zhao D, Asara J, Li W, Shi H, Caldwell R, Akrit A, Huo Y. Inactivation of adenosine receptor 2A suppresses endothelial-to-mesenchymal transition and inhibits subretinal fibrosis in mice [Dataset]. Dryad (2024).

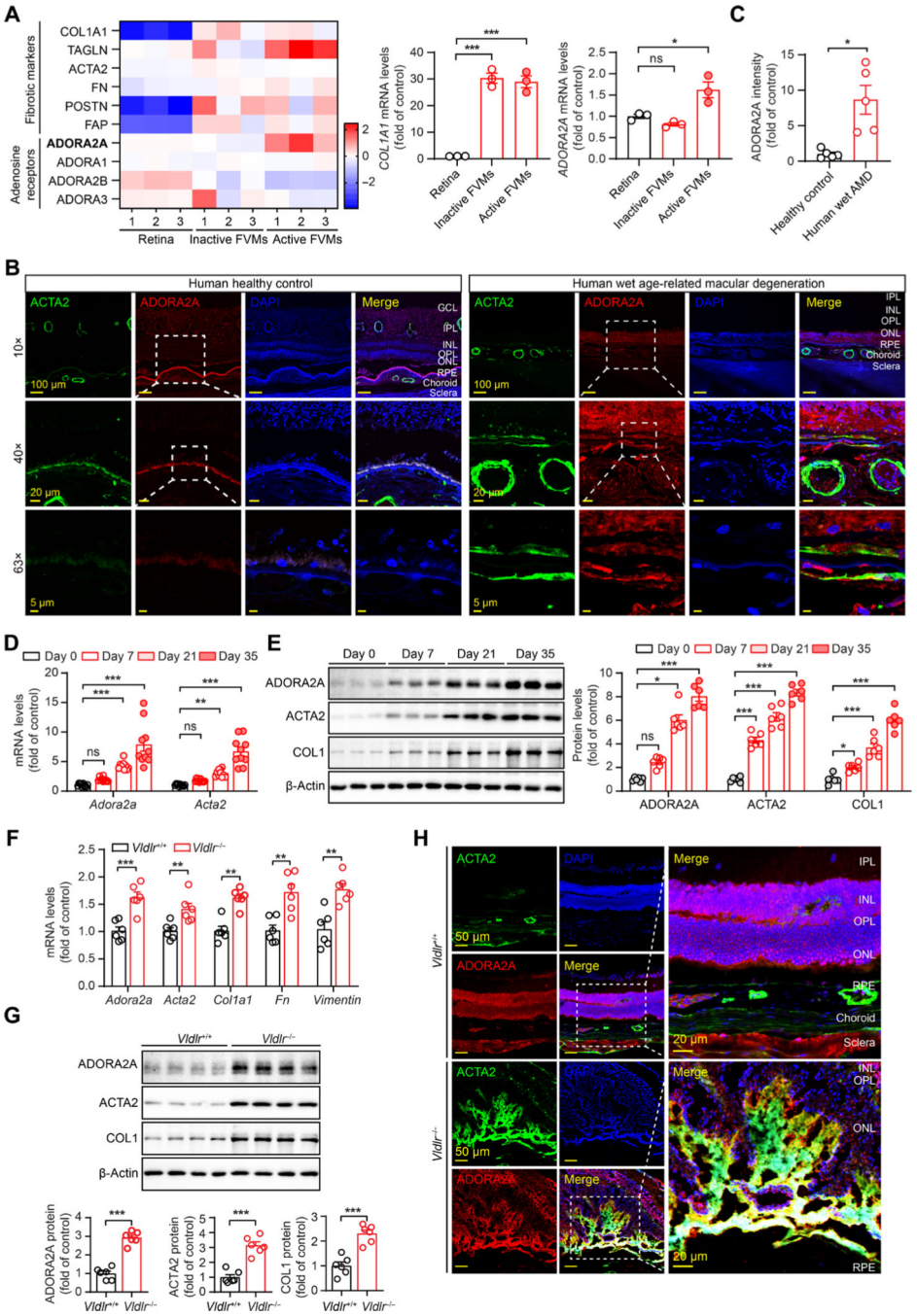

Fig. 1. ADORA2A expression is increased in the retinas of humans with wet AMD and rodents with subretinal fibrosis.

(**A**) Heatmap showing the gene expression of fibrotic markers and adenosine receptors in FVMs in patients with PDR. The data are from a reanalysis of the reported microarray dataset. $n = 3$. (**B** and **C**) Representative and quantification immunostaining of ADORA2A and ACTA2 in the retinas of humans with wet AMD and healthy individuals. DAPI, 4′,6-diamidino-2-phenylindole. Scale bars, 100 or 20, or 5 μm. $n = 5$. (**D**) qRT-PCR analysis of the mRNA expression of *Adora2a* and *Acta2* in RPE/choroid complex collected from

C57 mice at days 0, 7, 21, and 35 after laser photocoagulation. $n = 10$. (**E**) Representative Western blots and their quantification showing indicated protein expression in RPE/choroid complex collected from C57 mice at days 0, 7, 21, and 35 after laser photocoagulation. $n = 6$. (**F**) qRT-PCR analysis of the mRNA expression of indicated genes in RPE/choroid complex collected from *Vldlr*$^{-/-}$ and *Vldlr*$^{+/+}$ mice at 16-week-old age. $n = 6$. (**G**) Representative Western blots and their quantification showing indicated protein expression in RPE/choroid complex collected from *Vldlr*$^{-/-}$ and *Vldlr*$^{+/+}$ mice at 16-week-old age. $n = 6$. (**H**) Representative immunostaining of ADORA2A and ACTA2 on cross sections of the retina from *Vldlr*$^{-/-}$ and *Vldlr*$^{+/+}$ mice at 16-week-old age. Statistical analysis was performed using Kruskal-Wallis test (D and E), unpaired two-tailed *t* test (C, F, and G), and one-way ANOVA followed by a Bonferroni test (A and E). Data are means ± SEM. ns, no significance; $*P < 0.05$; $**P < 0.01$; $***P < 0.001$ for indicated comparisons.

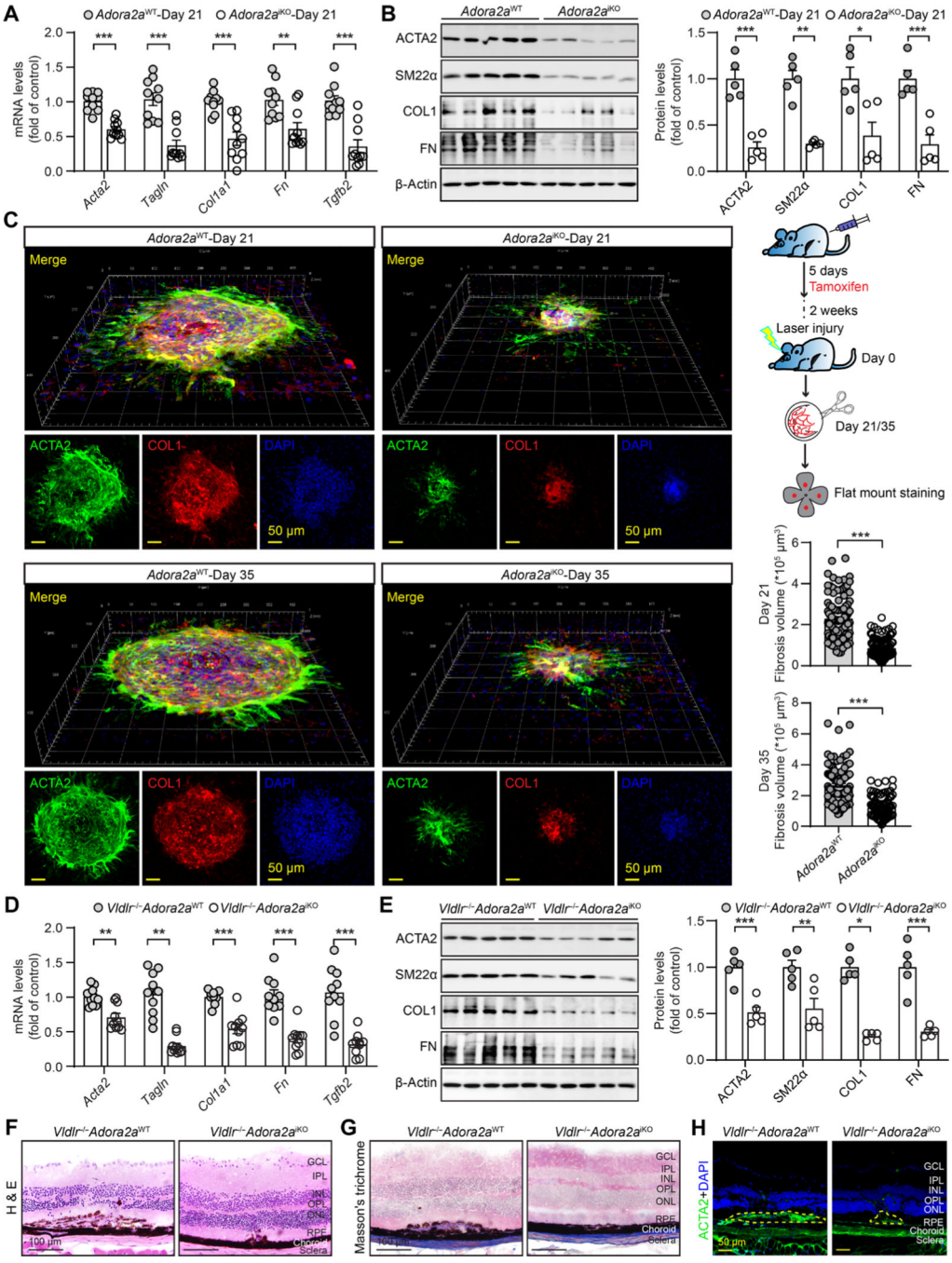

Fig. 2. Global *Adora2a* knockout suppresses subretinal fibrosis in laser injury–induced CNV mice and *Vldlr*$^{-/-}$ mice.

(**A**) qRT-PCR analysis of mRNA expression for the indicated genes in RPE/choroid complex collected from *Adora2a*^{WT} and *Adora2a*^{iKO} mice at day 21 after laser photocoagulation. n = 10. (**B**) Representative Western blots and their quantification showing indicated protein expression in RPE/choroid complex collected from *Adora2a*^{WT} and *Adora2a*^{iKO} mice at day 21 after laser photocoagulation. n = 5. (**C**) Representative images and quantification of immunostaining for acTa2 and col1 in RPE/choroid complex flat mount of *Adora2a*^{WT}

and *Adora2a*^{iKO} mice at day 21 or day 35 after laser photocoagulation. Scale bar, 50 μm. Four laser burns per eye, $n = 11$ to 14 mice per group. (**D**) qRT-PCR analysis of mRNA expression for the indicated genes in RPE/choroid complex collected from *Vldlr*$^{-/-}$*Adora2a*^{WT} and *Vldlr*$^{-/-}$*Adora2a*^{iKO} at 16-week-o ld age. $n = 10$. (**E**) Representative Western blots and their quantification showing indicated protein expression in RPE/choroid complex collected from *Vldlr*$^{-/-}$*Adora2a*^{WT} and *Vldlr*$^{-/-}$*Adora2a*^{iKO} mice at 16-week-old age. $n = 5$. (**F**) Representative hematoxylin and eosin (H&E)–stained cross sections of the retina from *Vldlr*$^{-/-}$*Adora2a*^{WT} and *Vldlr*$^{-/-}$*Adora2a*^{iKO} mice at 16-week-o ld age. Scale bar, 100 μm. $n = 5$. (**G**) Representative Masson's trichrome–stained cross sections of the retina from *Vldlr*$^{-/-}$*Adora2a*^{WT} and *Vldlr*$^{-/-}$*Adora2a*^{iKO} mice at 16-week-old age. Scale bar, 100 μm. $n = 5$. (**H**) Representative ACTA2 immunostaining on cross sections of the retina from *Vldlr*$^{-/-}$*Adora2a*^{WT} and *Vldlr*$^{-/-}$*Adora2a*^{iKO} mice at 16-week-old age. Scale bar, 50 μm. $n = 5$. Statistical analysis was performed using Mann-Whitney test (A to E) and unpaired two-tailed *t* test (A, B, D, and E). data are means ± SEM. $*P < 0.05$; $**P < 0.01$; $***P < 0.001$ for indicated comparisons.

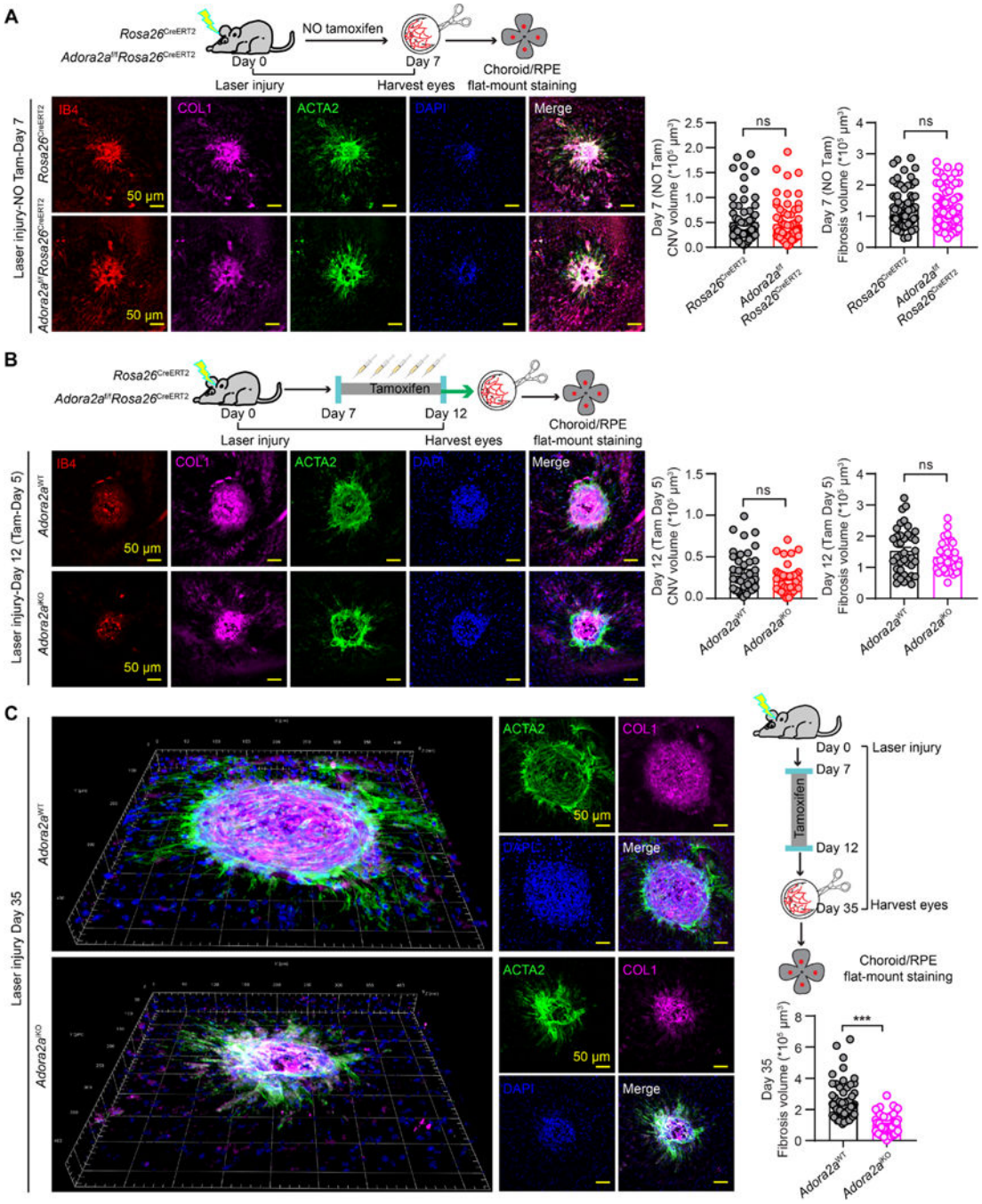

Fig. 3. The inhibitory effect of *Adora2a* deletion on subretinal fibrosis is largely independent of its antiangiogenic effect.

(**A**) Representative images and quantification of immunostaining for isolectin B4 (IB4, CNV), ACTA2, and collagen I (COL1, fibrosis) in RPE/choroid complex flat mount of *Rosa26*$^{\text{CreERT2}}$ and *Adora2a*$^{\text{f/f}}$*Rosa26*$^{\text{CreERT2}}$ mice without tamoxifen injection at day 7 after laser photocoagulation. Scale bar, 50 μm. Four laser burns per eye, $n = 8$ mice per group. (**B**) Representative images and quantification of immunostaining for IB4, ACTA2, and col1 in RPE/choroid complex flat mount of *Adora2a*$^{\text{WT}}$ and *Adora2a*$^{\text{iKO}}$ mice with

five consecutive tamoxifen injections at day 12 after laser photocoagulation. Scale bar, 50 μm. Four laser burns per eye, $n = 5$ mice per group. (**C**) Representative images and quantification immunostaining for ACTA2 and COL1 of RPE/choroid complex flat mount of *Adora2a*^{WT} and *Adora2a*^{iKo} mice with five consecutive tamoxifen injections at day 35 after laser photocoagulation. Scale bar, 50 μm. Four laser burns per eye, $n = 8$ mice per group. Statistical analysis was performed using Mann-Whitney test (A to C). Data are means ± SEM. ***$P < 0.001$ for indicated comparisons.

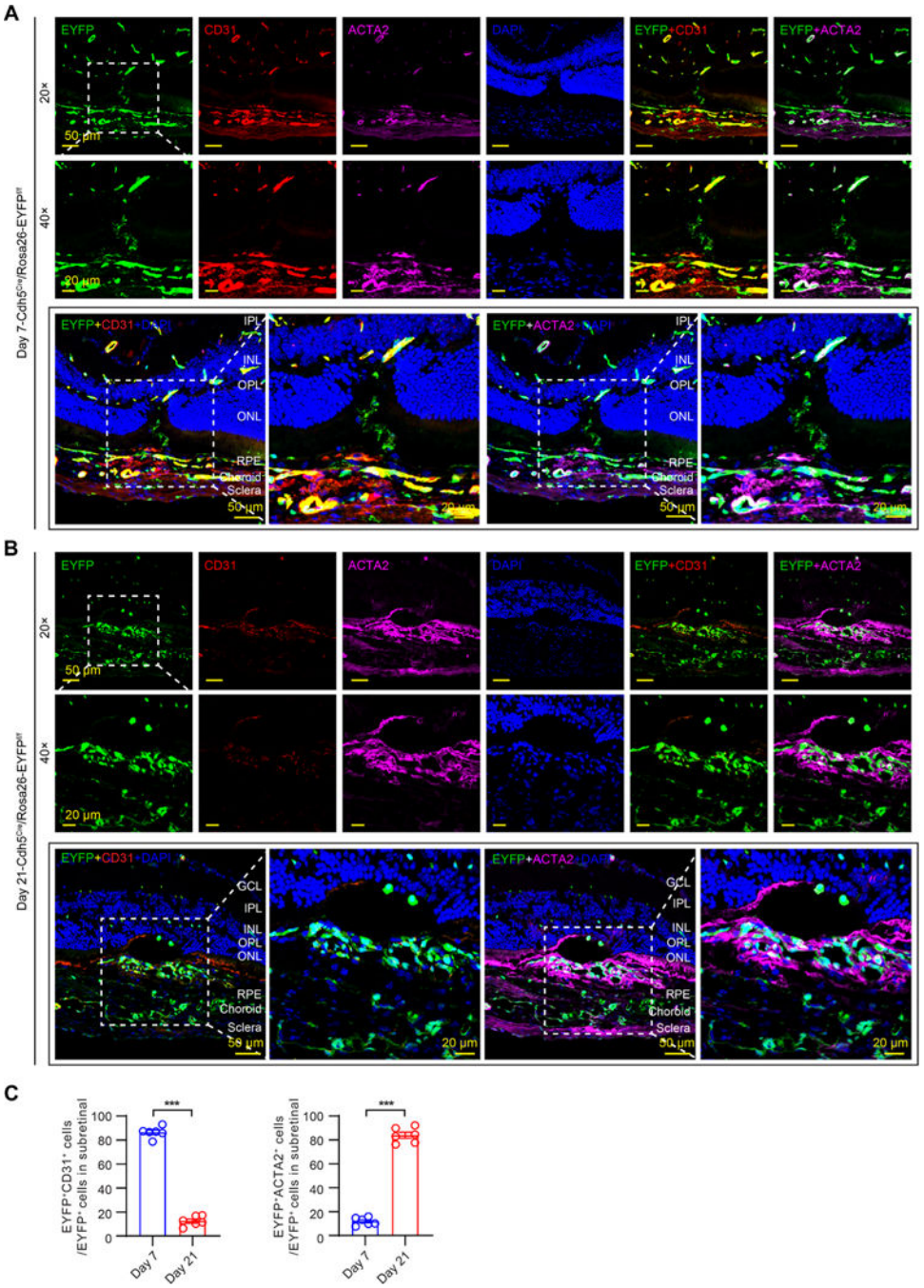

Fig. 4. Endothelial cells participate in the development of laser-induced subretinal fibrosis.

(**A**) Representative images of cd31 and acTa2 immunostaining on the cross section of retinas from EC lineage tracing mice *Cdh5*^{Cre}/*Rosa26*-EYFP$^{f/f}$ mice at day 7 after laser photocoagulation. Scale bars, 50 or 20 μm. Four laser burns per eye, $n = 6$ mice per group. (**B**) Representative images of cd31 and acTa2 immunostaining on the cross section of retinas from EC lineage tracing mice *Cdh5*^{cre}/*Rosa26*-EYFP$^{f/f}$ mice at day 21 after laser photocoagulation. Scale bars, 50 or 20 μm. Four laser burns per eye, $n = 6$ mice per group. (**C**) Quantification of CD31^{+}EYFP^{+} and ACTA2^{+}EYFP^{+} cells of images immunostained

with CD31 and ACTA2 from *Cdh5*^{Cre};*Rosa26*-EYFP$^{f/f}$ mice at days 7 and 21 after laser injury. $n = 6$ mice per group. Statistical analysis was performed using unpaired two-tailed t test. Data are means ± SEM. ***$P < 0.001$.

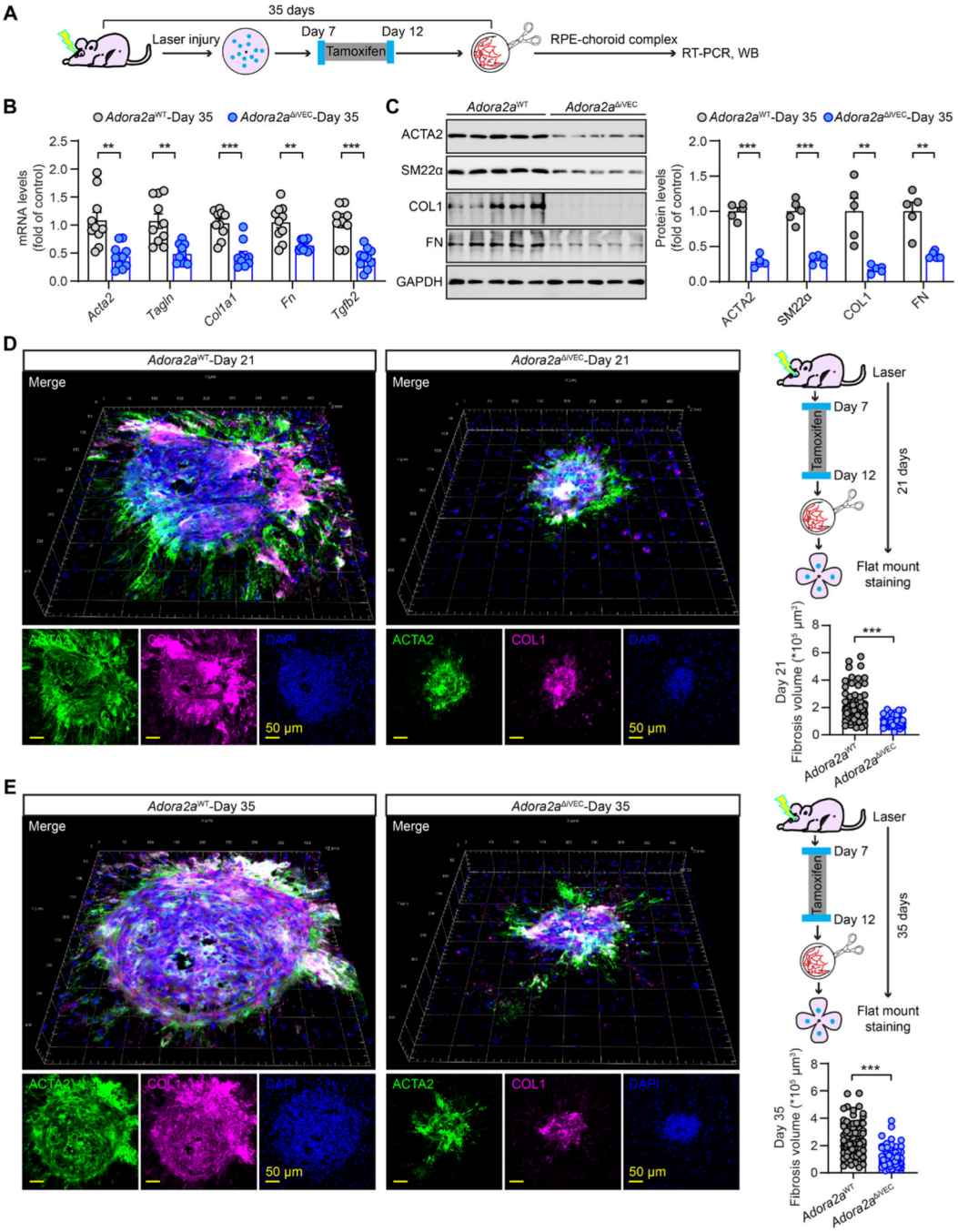

Fig. 5. Endothelial *Adora2a* participates in the development of laser-induced subretinal fibrosis.

(**A**) Schematic illustration of laser injury model in inducible EC *Adora2a*-deficient mice. (**B**) qRT-PCR analysis of the mRNA expression of indicated genes in RPE/choroid complex collected from *Adora2a*^{WT} and *Adora2a*$^{\Delta iVEC}$ mice at day 35 after laser photocoagulation. $n = 10$. (**C**) Representative Western blots and their quantification showing indicated protein expression in RPE/choroid complex collected from *Adora2a*^{WT} and *Adora2a*$^{\Delta iVEC}$ mice at day 35 after laser photocoagulation. $n = 5$. (**D** and **E**) Representative images and quantification of acTa2 and col1 immunostaining in RPE/choroid complex flat mount of

Adora2a^{WT} and *Adora2a*$^{\Delta iVEC}$ mice at day 21 or day 35 after laser photocoagulation. Scale bar, 50 μm. Four laser burns per eye, $n = 9$ to 12 mice per group. Statistical analysis was performed using Mann-Whitney test (B, D, and E) and unpaired two-tailed *t* test (B and C). Data are means ± SeM. $^{**}P < 0.01$; $^{***}P < 0.001$ for indicated comparisons.

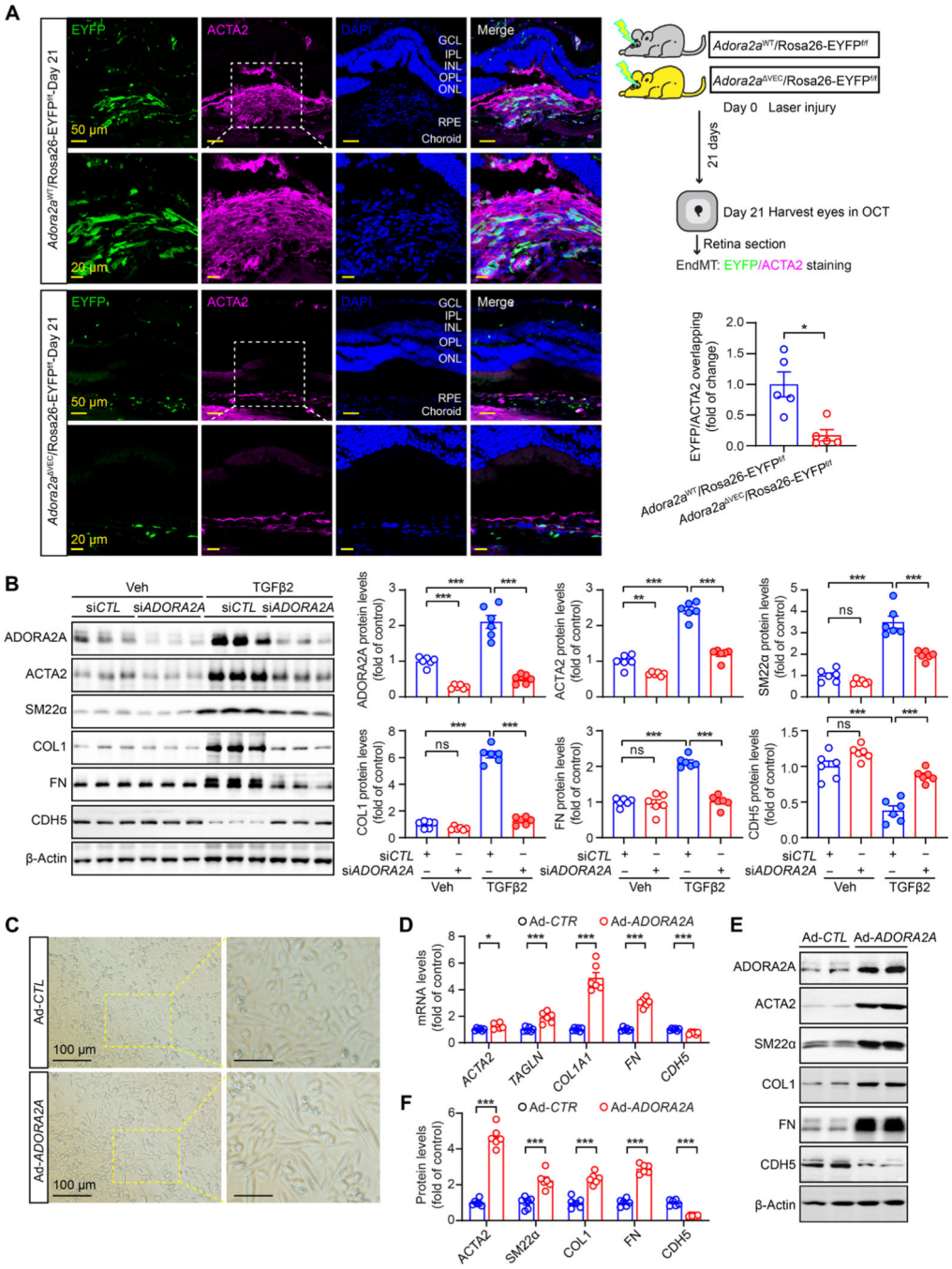

Fig. 6. EC ADORA2A promotes the process of endothelial-to-mesenchymal cell transition in vivo and in vitro.

(**A**) Representative images of ACTA2 immunostaining on cross section of retinas from *Adora2a*^{WT}/*Rosa26*-EYFP$^{f/f}$ and *Adora2a*$^{\Delta VEC}$/*Rosa26*-EYFP$^{f/f}$ mice at day 21 after laser photocoagulation. Scale bars, 50 or 20 μm. Four laser burns per eye, $n = 5$ mice per group. (**B**) Representative Western blots and quantification of indicated protein expression in hCECs transfected with control or *ADORA2A* siRNA for 24 hours and treated with hTGFβ2 (10 ng/ml) for 5 days. $n = 6$. Veh, vehicle. (**C**) Representative images of hCECs

infected with control or *ADORA2A* adenovirus for 5 days. Scale bar, 100 μm. (**D**) qRT-PCR analysis of the mRNA expression of indicated genes in hCECs infected with control or *ADORA2A* adenovirus for 5 days. $n = 6$. (**E**) Representative Western blots of indicated protein expression in hCECs infected with control or *ADORA2A* adenovirus for 5 days. (**F**) Quantification of Western blots for the indicated proteins in hCECs infected with control or *ADORA2A* adenovirus for 5 days. $n = 6$. Statistical analysis was performed using Mann-Whitney test (a), unpaired two-tailed *t* test (D and F), and two-way ANOVA followed by a Tukey post hoc analysis (B). Data are means ± SEM. $*P < 0.05$; $**P < 0.01$; $***P < 0.001$ for indicated comparisons.

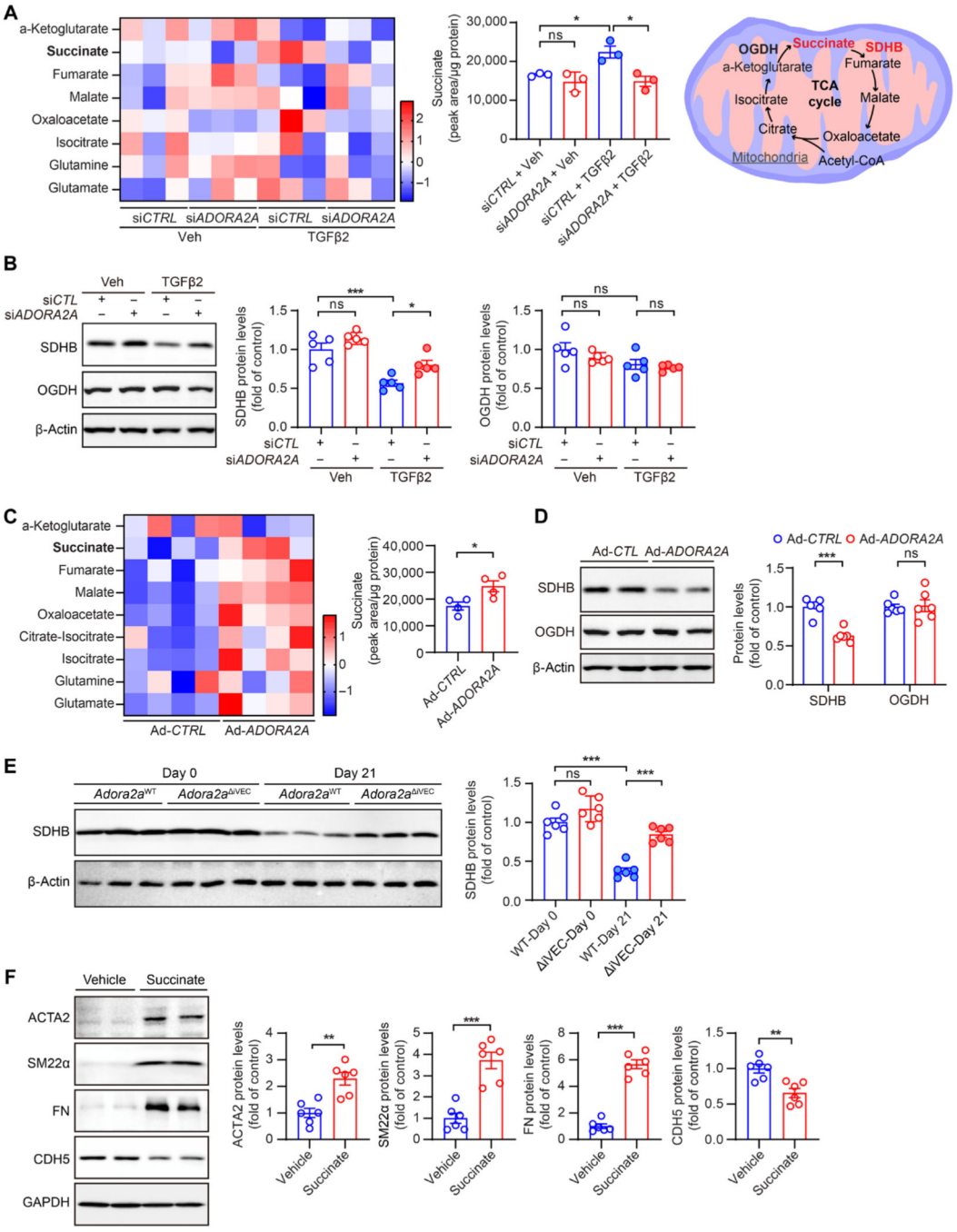

Fig. 7. ADORA2A mediates the SDHB-succinate signaling pathway to regulate EndMT in hCECs.

(**A**) Heatmap showing the metabolites in the TCA cycle pathway and quantification data of succinate amount in hCECs transfected with control or *ADORA2A* siRNA and treated with hTGFβ2 (10 ng/ml) for 48 hours. $n = 3$. (**B**) Representative Western blots and quantification of indicated protein expression in hCECs transfected with control or *ADORA2A* siRNA and treated with hTGFβ2 (10 ng/ml) for 5 days. $n = 5$. (**C**) Heatmap showing the metabolites in the TCA cycle pathway and quantification data of succinate

amount in hCECs infected with control or *ADORA2A* adenovirus for 48 hours. $n = 4$. (**D**) Representative Western blots and quantification of indicated protein expression in hCECs transfected with control or *ADORA2A* adenovirus for 5 days. $n = 5$. (**E**) Representative Western blots and quantification of indicated protein expression in RPE/choroid complex collected from $Adora2a^{WT}$ and $Adora2a^{\Delta iVEC}$ mice at day 21 after laser photocoagulation or noninjured mice. $n = 6$. (**F**) Representative Western blots and quantification of indicated protein expression in hCECs treated with vehicle or succinate (10 mM) for 5 days. $n = 6$. Statistical analysis was performed using unpaired two-tailed *t* test (c, d, and F) and two-way anoVa followed by a Tukey post hoc analysis (a, B, and e). Data are means ± SeM. $*P < 0.05$; $**P < 0.01$; $***P < 0.001$ for indicated comparisons.

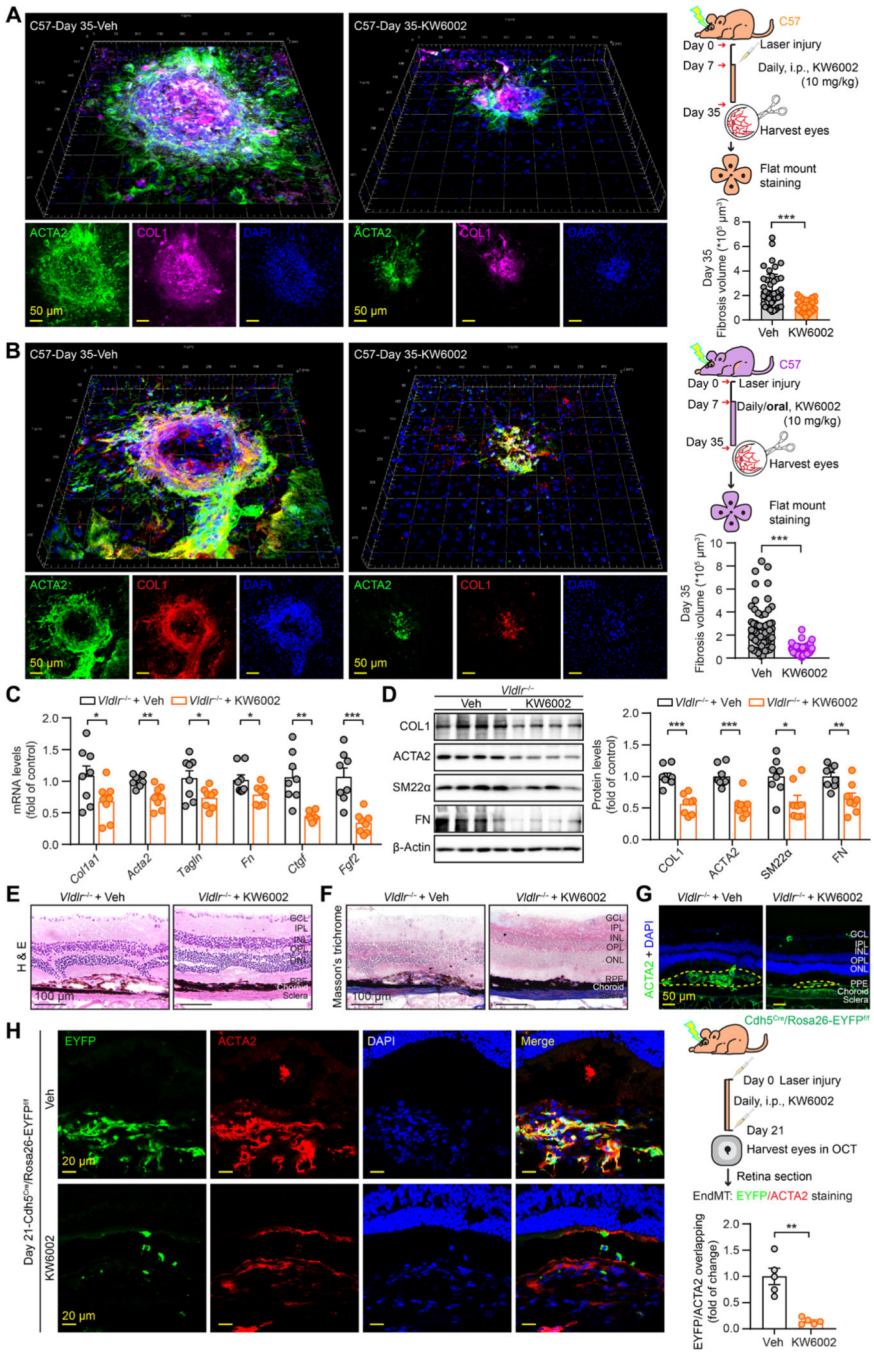

Fig. 8. *Adora2a* antagonist KW6002 suppresses subretinal fibrosis in laser injury–induced CNV mice and *Vldlr*$^{-/-}$ mice and inhibits EndMT in laser-injured EC lineage tracing mice.

(**A**) Schematic illustration, representative images, and quantification of ACTA2 and COL1 immunostaining in RPE/choroid complex flat mount of C57 mice treated with KW6002 (10 mg/kg) or vehicle by intraperitoneal injection at day 35 after laser photocoagulation. The treatment started from days 7 to 35 after laser photocoagulation. Scale bar, 50 μm. Four laser burns per eye, $n = 7$ or 8 mice per group. (**B**) Schematic illustration, representative images, and quantification of ACTA2 and COL1 immunostaining in RPE/choroid complex

flat mount of C57 mice treated with KW6002 (10 mg/kg) or vehicle by oral administration at day 35 after laser photocoagulation. The treatment started from days 7 to 35 after laser photocoagulation. Scale bar, 50 μm. Four laser burns per eye, $n = 7$ or 8 mice per group. (**C**) qRT-PCR analysis of the mRNA expression of indicated genes in RPE/choroid complex collected from *Vldlr*$^{-/-}$ mice treated with vehicle or KW6002. $n = 8$. Representative Western blots and their quantification showing indicated protein expression in RPE/choroid complex collected from *Vldlr*$^{-/-}$ mice treated with vehicle or KW6002. $n = 8$. (**E**) Representative H&E-stained cross sections of the retina from *Vldlr*$^{-/-}$ mice treated with vehicle or KW6002. Scale bar, 100 μm. $n = 5$. (**F**) Representative Masson's trichrome–stained cross sections of the retina from *Vldlr*$^{-/-}$ mice treated with vehicle or KW6002. Scale bar, 100 μm. $n = 5$. (**G**) Representative ACTA2 immunostaining on cross sections of the retina from *Vldlr*$^{-/-}$ mice treated with vehicle or KW6002. Scale bar, 50 μm. $n = 5$. (**H**) Representative images and quantification of ACTA2 immunostaining on the cross section from *Cdh5*^{Cre}/*Rosa26*-EYFP$^{f/f}$ mice treated with vehicle or KW6002 at day 21 after laser photocoagulation. The treatment started on the same day as laser photocoagulation. Scale bars, 20 μm. Four laser burns per eye, $n = 5$ mice per group. Statistical analysis was performed using Mann-Whitney test (A to D) and unpaired two-tailed *t* test (C, D, and H). Data are means ± SEM. $*P < 0.05$; $**P < 0.01$; $***P < 0.001$ for indicated comparisons.